Efficient Spin-Direction Coupling between Circular Polarized Electric and Magnetic Dipoles and Photonic Modes

Tingting Zhai, Matteo Mazzola, Demetrio Macias, Rafael Salas-Montiel

To cite this version:

Tingting Zhai, Matteo Mazzola, Demetrio Macias, Rafael Salas-Montiel. Efficient Spin-Direction Coupling between Circular Polarized Electric and Magnetic Dipoles and Photonic Modes. Advanced Quantum Technologies, 2022, 6 (2), pp.2200126. ⟨10.1002/qute.202200126⟩. ⟨hal-04014132⟩

HAL Id: hal-04014132
https://hal.science/hal-04014132v1

Submitted on 3 Mar 2023

Efficient spin-direction coupling between circular polarized electric and magnetic dipoles and photonic modes

Tingting Zhai, Matteo Mazzola, Demetrio Macias, and Rafael Salas-Montiel*

Laboratory Light, nanomaterials and nanotechnologies - L2n CNRS EMR 7004, Université de Technologie de Troyes, 10004 Troyes, France

*Corresponding author: rafael.salas@utt.fr

Abstract

Integrated single photon sources are essential elements in quantum technology applications such as computing, simulation, communication, metrology and in quantum photonic neural networks. The directional radiation and scattering of integrated single-photon sources play a crucial role in light manipulation, which relies on the electric and magnetic dipole moments of the emitter sources. Although clever physical insights and designer intuition strategies have been successfully applied in the development of integrated sources, inverse design strategies could enhance its performance. Inverse strategies such as topology optimization produce optimized geometries for nanophotonic devices that maximize its performance. Recently, topology-optimized couplers for on-chip single-photon sources were designed to efficiently couple light between a photonic mode in a waveguide and a single-photon source, assumed to be an electric dipole oriented along one axis. However, the superposition of orthogonal electric and magnetic dipoles can also be harnessed due to the additional degrees of freedom via their interference. In this work, we extended the topology optimization to couplers that enhance spin-direction coupling of circularly polarized, Huygens, and Janus dipoles. We demonstrated that topology optimization not only increases the light coupling to a desire mode but also enhances the electric and magnetic local density of states by the modification of the electromagnetic environment while maintaining the amplitude and phase relation between the orthogonal dipoles for unidirectional coupling. Currently, coupling efficiency and enhanced LDOS of up to 88%, 94%, and 93 % and up to 9.4, 18.6, and 14.9 are obtained for the circular polarized, Huygens, and Janus dipoles, respectively. The adjoint topology optimization improves the performances of 3D integrated photonic devices.

Introduction

Integrated single photon sources are essential integrated photonic components within a full integrated quantum photonic circuit. They provide the necessary generation of individual photons for further single and multiple states processing and detection. Such components will form the next generation of photonic circuits that will open the way to quantum photonic technologies. Practical quantum photonic technologies such as computing, simulation, communication, and metrology as well as recent advances in quantum optical neural networks are envisioned with the use of integrated photonic circuits [1]. Among the single photon sources available, quantum emitters are promising sources for quantum networks [2] as they can reach near-optimal emission production of on-demand and single indistinguishable photons [3]. In addition to quantum dot emitters, quantum emitters embedded in 2D transition metal dichalcogenides have shown to present unique properties [4] and have been integrated in photonic structure [5]. It is known that the rate of emission of photons by quantum emitters is not an intrinsic property and can therefore be enhanced via the modification of their local environment or equivalently, via the modification of the local density of states (LDOS) [6]. The coupling of quantum emitters to photonic microcavities with optimized spatial and spectral overlap has been proven to increase the rate of emission [7]. In addition to the coupling of quantum emitters to photonic structures that enhance the Purcell effect, the emission radiation is directed into a particular direction for further processing [8,9]. In this regard, integrated photonics is an excellent platform for both increasing the LDOS and collection efficiency. Quantum dots emitters coupled to planar nanobeam waveguide [10] and electrically contacted planar photonic crystal waveguide membrane has demonstrated to produce indistinguishable and efficient single photons [11]. Hybrid structure consisting of a high-index layer placed on top of an ion-exchanged glass waveguide has also proved the enhancement of emission of quantum emitters [12]. Moreover, plasmonic waveguides have also been employed for the enhancement of the emission of quantum emitters in quantum technologies [13]. However, all these integrated photonic structures were developed following physical insights and designer’s intuition, dealing with predefined configurations. As the quantum integrated circuits scale up to large bandwidth, multi-frequency applications, nonlinear phenomena, and dense integration, the prototypical approach poses a challenge of increasing complexity [14]. Therefore, controlling the propagation of guided light via fast and robust near field interference between polarization components of a single photon sources is required [15]. As an alternative candidate, inverse design strategies such as topology optimization could reshape the landscape of available nanophotonic structures that have more forgiving design rules with the goal of maximizing the performance [16]. Recently, a nanoscale light extractor was designed using adjoint-optimization methods to enhance by 35 times the broadband emission of nitrogen vacancy (NV) centers in diamond. The extractor collects the emission into radiative modes (i.e., to free space), directing the light into a narrow cone that can be collected with low numerical aperture optical systems with 40% collection efficiency [17]. Another extractor, designed using inverse design, enhances by 14 times the emission of NV centers in diamond [18]. Topology-optimized couplers for on-chip single-photon sources were designed to efficiently couple light emission of a single-photon emitter to a photonic mode in a waveguide. The emitter is however, assumed to be an electric dipole oriented along one axis [19].

Circular polarized dipoles, together with Huygens and Janus dipoles, form the complete set of directional dipolar sources in the far- and near-field [20]. These dipoles are known to have a near-field directionality and can thus excite a guided mode in one direction only if placed in the vicinity of a waveguide. The near field directionality for the circularly polarized dipole is explained based on its spin angular momentum. This dipole is formed by the superposition of two orthogonal electric or magnetic dipole, 90° out of phase. The transverse spin is at the origin of the directional excitation of guided modes via spin-orbit coupling. This coupling is done by placing the dipole in regions where the modes show local circular polarization [21]. In the Huygens dipole, an electric and a magnetic dipoles are orthogonal to each other and in phase while in the Janus dipole the orthogonal electric and magnetic dipoles have a 90° phase shift. These combinations provide directionality in both the far- and near- fields. The Janus dipole is said to have two “faces”: one face couples into the mode, while the other is noncoupling [22]. Although these dipoles are highly directional and have unique properties for side coupling to guided modes, their coupling efficiency is low, and their local densities of states (LDOS) are weakly enhanced due to the side coupling.

In this work, we thus extended the topology optimization to couplers with circularly polarized dipoles as well as Huygens and Janus dipoles. We demonstrated that topology optimization not only increases the light coupling to a desire mode of an output waveguide but also it enhances the LDOS. Specifically, we calculate the coupling efficiency and LDOS enhancement of a topology optimized structure compared to a non-optimized structure.

Methods and Materials

We used the adjoint method implemented by Meep [23] to systematically design a compact silicon photonic structure that maximize a fraction of the radiation emission of a single-photon emitter into the fundamental mode of the output silicon waveguide (Fig. 1). The single-photon emitter is modeled as a dipole as described in Table I and thus, we designed the structure to maximize the coupling efficiency into the fundamental mode of the output waveguide.

Table I. Used sources and their respective electric and magnetic dipoles.

	Circular polarized source	**Huygens' source**	**Janus source**	
			noncoupling	**coupling**
Electric dipole	**p** = (1, 0, 1i)	**p** = (0, 0, 1)	**p** = (-1, 0, 0)	**p** = (+1, 0, 0)
Magnetic dipole	**m** = (0, 0, 0)	**m** = (0, 1c, 0)	**m** = (0, 1ic, 0)	**m** = (0, 1ic, 0)

In the simulations, the computational domain is a rectangle of size 13 µm by 7 µm, including 1-µm-thick perfectly matched layers (PML) around the four boundaries. We use a grid mesh of 40 (pixels.µm^{-1}), that is 1/40=0.025 µm. The optimization domain is 3 µm x 3 µm and has thus 120 by 120 design parameters. The right-hand side of the design region is connected to a photonic waveguide of width 0.5 µm and length 4 µm and refractive index n_2 =3.4. The outside region is silicon dioxide with index of refraction n_1 = 1.44 [24] (Fig. 1b). We specify a characteristic length scale of the structure in the domain a = 1 µm. Then, a wavelength of λ = 1.55 µm corresponds to a frequency 0.64516 (i.e., a/λ = 1µm/1.55µm = 0.64516). Initially a dipole is placed at the center of the design region.

The objective function is defined by:

$$\eta_i(\mathbf{r_0}, \omega) = \frac{|a_i(\mathbf{r_0},\omega)|^2}{P_{l,in}(\mathbf{r_0},\omega)} \text{.... (1)},$$

where $a_i(\mathbf{r}_0, \omega)$ is the expansion coefficient of the *i*-th mode at the output waveguide. The expansion coefficient is given by an overlap integral over a cross-section A, $a_i(\mathbf{r}_0, \omega) = < \Omega_i \mid \Omega >$, where Ω_i is the eigenmode profile corresponding to the *i*-th eigenmode at the output waveguide and Ω is the total fields. $P_{l,in}$ is the power emitted by the dipole placed at $\mathbf{r}_0$ and oriented along the direction $l \in \{x, y, z\}$. This input power was calculated by calculating the Poynting flux power transmitted out of a box surrounding the dipole.

The optimization is done within a spectrum centered at frequency 0.64516 with a frequency width of 0.129, from 0.58 to 0.71 in units of (a/λ). This means at the central wavelength λ = 1.55 μm, from 1.408 μm to 1.724 μm. In other words, we seek to maximize the fraction of the power emitted by the source into the fundamental mode of the output waveguide in a spectrum centered at 0.64516 with a frequency width of 0.129 in units of (a/λ).

In addition, we calculated the modification of the LDOS of the source placed in the topology-optimized structure. The total LDOS($\mathbf{r}_0$, ω) is given by the sum of the electric and magnetic contribution [25]. In FDTD, the electric LDOS is given by [26]:

$$\text{LDOS}_l\,(\mathbf{r_0},\omega) = -\frac{2}{\pi}\epsilon(\mathbf{r_0})Re\left[\frac{E_l(\mathbf{r_0},\omega)\mathbf{p}(\omega)^*}{|\mathbf{p}(\omega)|^2}\right], \qquad \dots (2)$$

where the subscript "l" indicates the oriented of the dipole, $l \in$ {x, y, z} and $|p(\omega)|^2$ is the spectrum of an impulsive point-dipole source $\mathbf{J}(\mathbf{r_0},t) = \mathbf{e_l}\,\delta(\mathbf{r}-\mathbf{r_0})p(t)$. However, this value in the denominator is cancelled as we are not interested in the absolute value of the LDOS, but rather in the relative enhancement of the LDOS relative to another structure. We thus obtained a normalized LDOS by dividing the LDOS in the optimized region by the LDOS of the same dipole placed in a non-optimized region (i.e., homogeneous design region with index n_2 = 3.4). This ratio is equivalent to the Purcell factor.

The size of the design region of 3 μm x 3 μm is chosen so that the dipole has multiple modes to interact with. The dipole interacts with the non-zero field components e_z, h_y, and e_x of the available modes to perform directionality and optimization. The optimization algorithm forces the amplitude and phase relationship of the dipoles to maximize the coupling efficiency into the fundamental mode. In our case, the fundamental mode has the main component of the magnetic field out-of-plane (i.e., component H_y). The dispersion relation of the output waveguide is plotted in Fig. 1d. At the central frequency 0.64516 (a/λ), the wavevector is 2.06 (2π μm^{-1}). The first-order mode is cut-off, which means that the output silicon waveguide is single mode at this frequency. The dispersion relation ω(**k**) for index-guided modes with even mirror symmetry in the y-direction was calculated with the use of MPB [27]. The gray region represents the light cone (n_1= 1.44) and encloses the radiative modes.

Although we treated the problem as a 2D one to reduce computational time and effort, the photonic structure can be extended to a 3D case. A way to treat a 3D structure is to map the 3D problem into an approximative 2D one by using the effective index method [28]. In this case thus, the index of refraction of the photonic structure is that of the effective index of the fundamental vertical slab mode. For 3D optimizations, we used a 2D optimization domain (i.e., a 2D material grid) and extruded the design into the vertical direction by transferring the optimization domain along all thickness of the silicon layer. The extrusion process consists of stretching the flat, 2D shape vertically to generate the 3D photonic device.

This design method is a convenient method for the optimization and for the fabrication of the device with standard planar fabrication tools such as electron beam lithography and reactive ion etching. We show the results of this approach in the supplementary information.

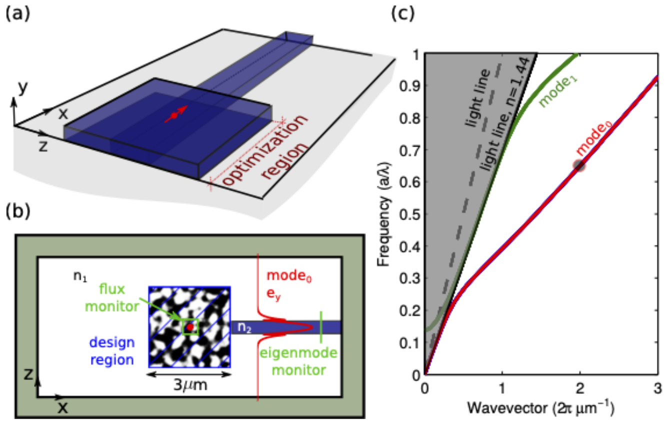

Figure 1. Topology optimization problem. (a) 3D schematic of the photonic structure with a square optimization region. (b) The 2D problem geometry where the 3 μm by 3 μm optimization region is seen. The right side of the optimization region is connected to the output port waveguide where the power coupled into the fundamental mode is calculated. The red profile is the calculated eigenmode at frequency 0.64516 (a/λ). The wavevector at this frequency is 2.06 (2π μm^{-1}). The dipole is represented by a red point and placed at the center of the optimization region. The light green box represents the flux monitor to calculate the power radiated by the dipole. The green region around the structure represents the PML. (c) Calculated dispersion relation of the output silicon waveguide.

To eliminate the optimization of topological structures with size features unattainable with current nanofabrication tools (i.e., standard electron beam lithography), we include nanofabrication constraints in the design region. Specifically, linear and nonlinear functional transform on the design parameters were included before projecting them onto the simulation domain. A conic filter was used to blur out features with size lower than a threshold with a minimum length of 0.09 μm.

The adjoint solver implemented in Meep is based on the density method and efficiently computes the gradient of an arbitrary function of the electromagnetic fields with respect to ε on a discrete spatial grid. In the density-based method, each pixel in the design region is either solid or void for high- and low-index materials, respectively. The design is gradually binarized with the application of a series of filters and projectors. One important aspect of this process is that the cost function and its gradient are continuous and thus differentiable. Moreover, the method involves two separate simulations: the first one is the "forward" simulation that computes the fraction of the power emitted by the dipole into the fundamental mode and the fields in the design region and the second simulation is the "adjoint" one that computes the fields in the design region with another special type of source distribution. The gradient of the objective function with respect to the design variables is obtained in a post-processing using the fields in the forward and adjoint simulations. After the calculation of the gradient, we finally run the optimization algorithm based on the method of moving asymptotes (MMA) available in the NLopt library [29,30]. The gradient values are used to update the material density distributions in the design region for the next iteration. Initially, the material distribution within the design region is random and varies within lower and upper bounds from 0 (i.e., $\epsilon_1 = n_1^2$) to 1 (i.e., $\epsilon_2 = n_2^2$). The permittivity at each grid cell is a design parameter denoted as $\epsilon(\rho) = \epsilon_1 + \rho(\epsilon_2 - \epsilon_1)$, $\rho \in [0,1]$. Further details on the adjoint method can be found in reference [31]. We run all processes for a number of n = 50 runs to statistically treat the modal collection efficiency and LDOS obtained through topology optimization.

We done this by computing the mean m and standard deviation σ of the objective solutions. The uncertainty is defined as $u = \sigma \cdot n^{-\frac{1}{2}}$(i.e., the standard error).

Results and discussion

To present the results of the optimization algorithm, we divide this section into three subsections, each of one presents the results of a particular source. The comparison between 2D and 3D topology-optimized photonic devices, influence of the design region size and position of the dipole source within the design region are also investigated, specifically in the supplementary materials. Finally, in the supplementary information, we plotted the results for single electric dipole oriented along x and z, and that for a magnetic dipole oriented along the y axis.

Circular polarized dipole source

Figure 2 shows the evolution of the design region as the method finds the best β-factor for one of the topology optimization realizations. The design region follows a rapid transformation from a random initial to a final optimized design. Indeed, we see that the final optimized design reaches its final form from iteration 35 (Fig. 2a). Correspondingly, the β-factor of the topology optimized photonic structure is shown in (Fig. 2b).

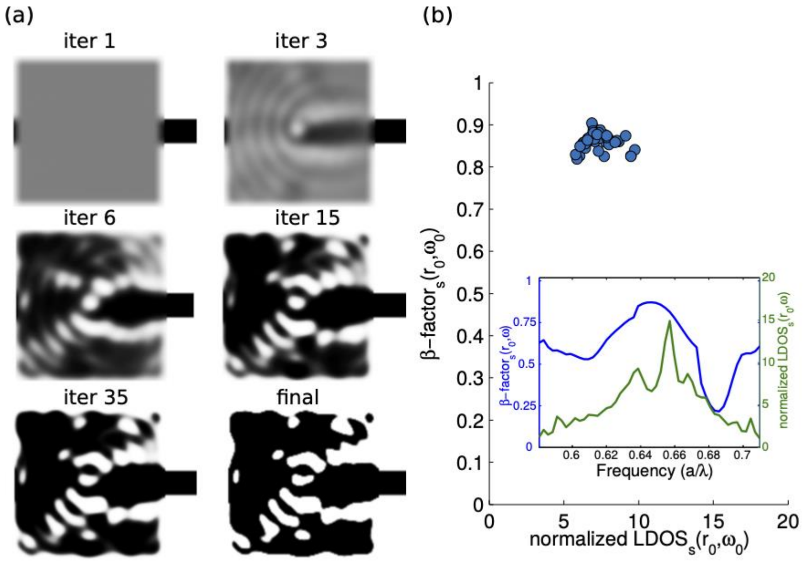

Figure 2. Topology optimization of the integrated circular polarized single photon source. (a) Evolution of the design region where the position $\mathbf{r}_0$ of the dipole is at the center of the 3 µm by 3 µm design region. (b) Scatter plot with circular markers at the locations specified by the enhancement of the local density of states (i.e., the Purcell factor) and the collection efficiency at frequency 0.64516(a/λ) for 50 optimization runs. Each optimization is done for a broad band spectrum centered at frequency 0.64516(a/λ) and with a width of 0.129. Inset: the collection efficiency and Purcell factor spectra for the optimization run number of 20.

For collection efficiency we obtain a minimum and maximum of 0.82 and 0.90, respectively. The mean and standard deviation are 0.86 and 0.019. In addition to the best collection efficiency (or β-factor), the optimized photonic structure enhances the LDOS compared to the LDOS in free space at frequency 0.64516(a/λ). For a number of n = 50 realizations, the minimum and maximum LDOS values are 5.8 and 9.7 with a mean of 7.2 and standard deviation of 0.94. The respective uncertainty is 0.13.

In figure 3, we show the distribution of the components of the electric and magnetic field propagating along the optimized structure as well as the absolute squared value of the electric field at the central frequency. We recall here that the algorithm is set to optimize the coupling into the fundamental mode of the output waveguide with out-of-plane magnetic field h_y.

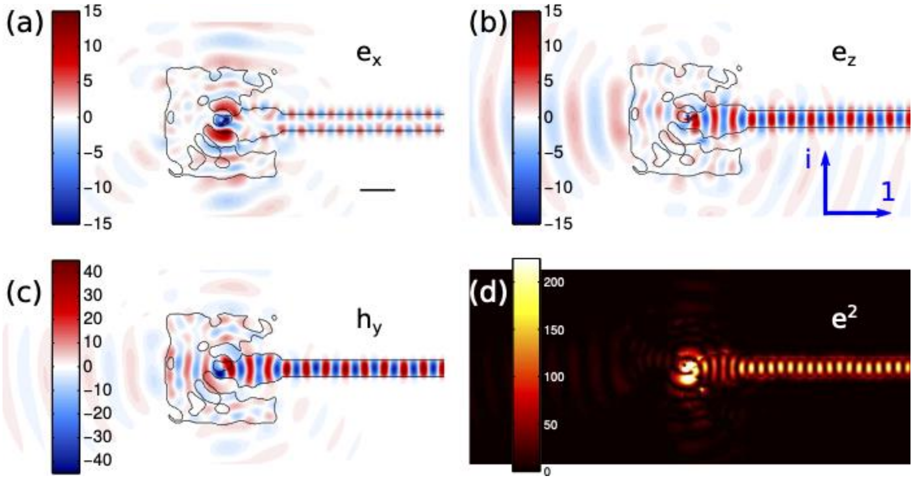

Figure 3. Distribution of the field along the topology optimized integrated single photon source. Propagation of (a) the x-component, (b) z-component of the electric field and (c) the y-component of the magnetic field along the optimized structure. (d) Distribution of the electric field squared. The scale bar is 500 nm in (a) and the inset in (b) shows the orientation of the dipoles. The frequency is 0.64516(a/λ).

The circular polarized dipole interacts with the y-even modes, which have non-zero field components e_z, h_y, and e_x. The p_x and p_z components of the dipole couple to the e_x and e_z components of the available modes. In a regular spin-directional coupling, when the dipole is placed in the near field of a waveguide modes, the interaction is done through the transverse spin angular momentum (SAM) density [32-34]. The transverse SAM is either positive or negative inside the waveguide and therefore, by placing the dipole at $\mathbf{r}_0 = (x_0, \pm z_0)$, the dipole excites the mode propagating along the ±x-axis (Fig. 4b).

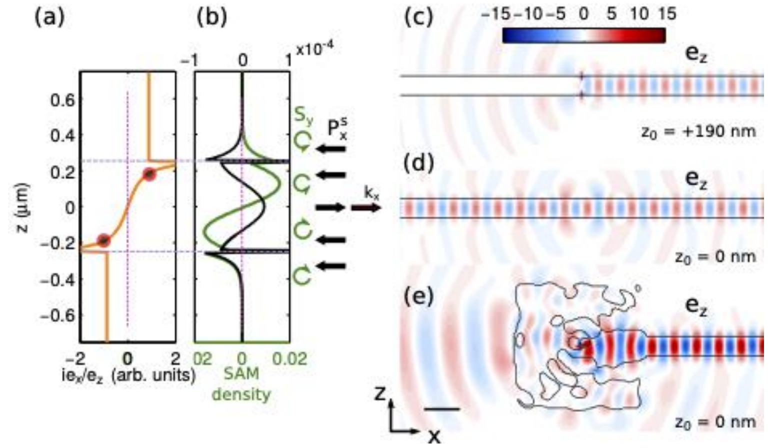

Figure 4. Eigenmode analysis and FDTD calculation of the spin-orbit coupling. (a) Distribution of the ratio between ie_x and e_z field components. The points in ie_x/e_z show the region where the amplitude of these two components is equal at $z_0 = \pm190$ nm. (b) Calculated distribution of the only nonzero components of the spin AM density S_e (i.e., S_y, the y-component, green solid line) and the spin momentum Ps_x. Distribution of the electric field for a circular polarized dipole placed at (c) $z_0 = 190$ nm and (d) $z_0 = 0$ in a straight waveguide, and (e) placed at the center of the topology optimized. Unidirectional coupling into the forward mode is obtained at the spin-orbit locking position in (c) and enhanced unidirectionality in the optimized structure (i.e., in (e)). The distributions are obtained at frequency 0.64516(a/λ) and the scale bar is 1 µm.

In optimized design, the topology is formed such that the field modes, specifically the component e_x and e_z have a fixed amplitude and phase relationship. In the topology-optimized region, the optimization starts first with the dipole in a design region supporting six modes. Because the dipole is placed at the center, the transverse SAM density is zero for all the modes (i.e., the electric part of the SAM $S_y = 0$). The emission is therefore coupled to both the forward and backward modes. One can see that the first iterations in the optimization generate a mirror that reflects the emission, coupled to the backward modes, to the +x-axis maximizing the collection efficiency.

Because the amplitude and phase relationship between the e_x and e_z components must be fixed for unidirectional emission, the algorithm enforces this relationship by surrounding the dipole in void and material parts, with some rotational symmetry. The dipole itself has rotational symmetry around the y-axis. The coupling efficiency of a topology optimized structure is three times higher than that with spin-orbit locking (see suppl. info.).

To investigate the influence of the size of the design region and the optimization with less available modes in the design region, we conducted optimizations with squared design regions of side 2.0 µm, 1.5µm, and 1.0 µm (i.e., 1.29λ, λ, and 0.64λ). In those cases, the available modes at frequency f = 0.64516 are 4, 3, and 2, respectively. We present in Table II the collection efficiencies into the fundamental mode for the different region side size.

The collection efficiencies decrease as the size of the design region decreases, 12% of the collection efficiency is lost when the side is reduced by a factor of two (i.e., for a region of size of 1.5µm by 1.5µm). A figure that shows the propagation of the electric field for optimized design regions of 2µm, 1.5µm, and 1µm can be found in suppl. info (Fig. S6). The reduction of the size of the design region to one-wavelength results in a collection efficiency of 73% and a Purcell factor of 10.3.

Table II. Collection efficiencies and Purcell factors for topology optimized regions with different sides.

Design region side (µm)	Collection efficiency	Purcell factor
3.0	0.88	9.4
2.0	0.77	7.4
1.5	0.76	5.9
1.0	0.73	10.3

In addition to the influence of the size of the design region, we also investigated the influence of the position of the dipole within the design region on the collection efficiency. Indeed, the topology optimizations in previous cases were done for a dipole placed at the center of the design region. We investigated four different random off-center positions of the dipole in a 3-µm-side design region (Table III). The corresponding electric field distributions and optimized design regions at frequency f = 0.64516 are shown in supplementary information.

Table III. Collection efficiency at f=0.64516 in units of (a/λ) for four different positions around the design region of the circular polarized dipole. Δx and Δz are the offset distance relative to the center of the design region.

Offset from the center	Δx (µm)	Δz (µm)	Collection efficiency	Purcell factor
0	0	0	0.88	10.1
1	-0.75	+0.75	0.85	8.2
2	+0.75	+0.75	0.92	9.2
3	-0.5	-1.0	0.94	7.8
4	+1.25	-0.5	0.90	2.65

Although the dipole is placed off-center, the TO leads to high collection efficiency (> 85%) into the fundamental mode while providing values of the Purcell factor comparable to that for the dipole placed at the center of the design region.

For 3D optimizations, we used a 2D optimization domain (i.e., a 2D material grid) and extruded the design into the vertical direction by transferring the optimization domain along all thickness of the silicon layer. The thickness of the silicon layer was fixed to 220 nm and the dipole was placed on top of the design region. The 3D topology optimization with a 2D design region yields collection efficiency as high as 84% and a Purcell factor of 33.6. The collection efficiency is comparable to that obtained in the effective 2D optimization. The Purcell factor increases as the effective mode volume decreases; indeed, the optical confinement is in 3D. The spin-direction coupling via topology optimization is viable in 3D photonic devices.

Huygens' dipole source

Figure 5 shows the topology optimized photonic structure. The minimum and maximum LDOS values are 6.3 and 9.7 with a mean of 7.2 and standard deviation of 0.77. The respective uncertainty is 0.1. For the β-factor we obtained a minimum and a maximum of 0.89 and 0.99, respectively. The mean and standard deviation are 0.98 and 0.04. In figure 5, we show the distribution of the components of the electric and magnetic field propagating along the optimized structure as well as the absolute squared value of the electric field at the central frequency. We recall here that the algorithm is set to optimize the coupling into the fundamental mode of the output waveguide with out-of-plane magnetic field h_y.

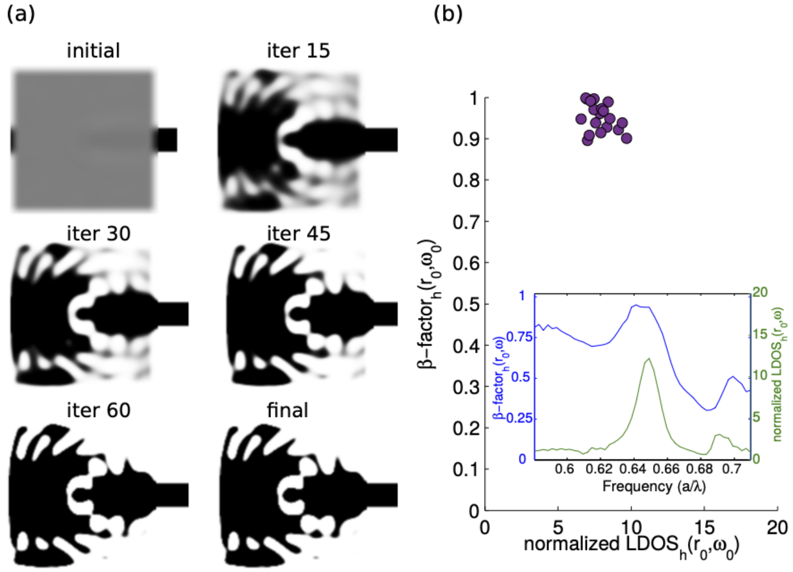

Figure 5. Topology optimization of the integrated Huygens' dipole. (a) Evolution of the design region. (b) Enhancement of the local density of states and collection efficiency corresponding to the optimized photonic structure on one of the topology optimization realizations. Inset: Purcell and collection efficiency spectra.

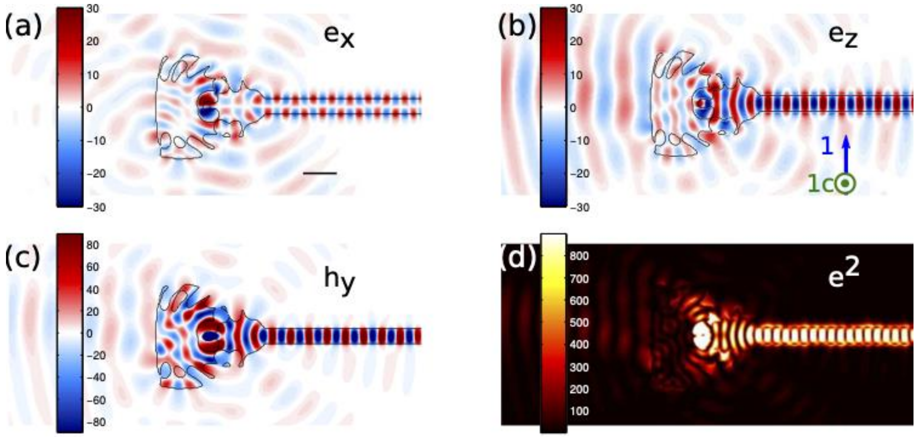

Figure 6. Distribution of the fields along the topology optimized integrated Huygens' dipole. Propagation of (a) the x- and (b) z-component of the electric field, real part. (c) Distribution of the y-component of the magnetic field and (d) squared electric field. The scale bar is 500 nm and the inset in (b) shows the orientation of the dipole. The frequency is 0.64516(a/λ).

The Huygens dipole produces a net power flow in each direction due to the relative amplitude and phase between the electric and magnetic dipoles. Here, the electric and magnetic dipoles are orthogonal and in-phase, which produces directionality when placed in the near field of a waveguide (Fig. S12b and d).

The coupling efficiency of a Huygens dipole placed at the center of the topology optimized region is more than one order of magnitude higher than that of the Huygens dipole placed in the near field of a waveguide, with an enhancement of about 15 (Fig. S12f).

In the Huygens dipole, the p_z and h_y components of the dipole couple to the transversal e_z and h_y components of the available modes. It does not involve coupling to the longitudinal x-component of the electric field. In optimized design, the topology is formed such that the field modes, specifically the component e_z and h_y have a fixed amplitude and phase relationship. The emission is therefore coupled to the forward modes but some of the radiation radiates at some angle. One can think that optimization generates a focusing structure to focus the light into the output waveguide, maximizing the collection efficiency. Because the amplitude and phase relationship between the e_z and h_y components must be fixed, the algorithm enforces this relationship by surrounding the dipole in material part, with some mirror-symmetry with respect to the z = 0 plane, as the Huygens dipole itself.

Finally, we conducted the effective 2D optimization (2D TO then 3D simulation with the geometry extruded in the vertical direction) with the Huygens dipole on the top of the optimization domain. We obtained a coupling efficiency of 72% and a Purcell factor of 22.8.

Janus dipole source: coupling and noncoupling faces

In table IV, we present the basic statistics for n = 50 realization of the Janus dipole source. Figure 7 shows the topology optimized photonic structure. We recall here that the algorithm is set to optimize the coupling into the fundamental mode of the output waveguide with out-of-plane magnetic field h_y.

Table IV. Basic statistics on n = 50 optimization runs for a Janus dipole source.

	noncoupling		**coupling**	
	LDOS	**Collection efficiency**	**LDOS**	**Collection efficiency**
min	5.9	0.91	6.9	0.85
max	15.6	1.0	14.6	1.0
mean	8.1	0.98	10.0	0.92
Std. deviation	1.7	0.03	1.85	0.04
uncertainty	0.24	0.005	0.26	0.005

It is interesting to note that the optimization algorithm works for the noncoupling face Janus dipole. The noncoupling face presents values comparable to that of the coupling Janus dipole.

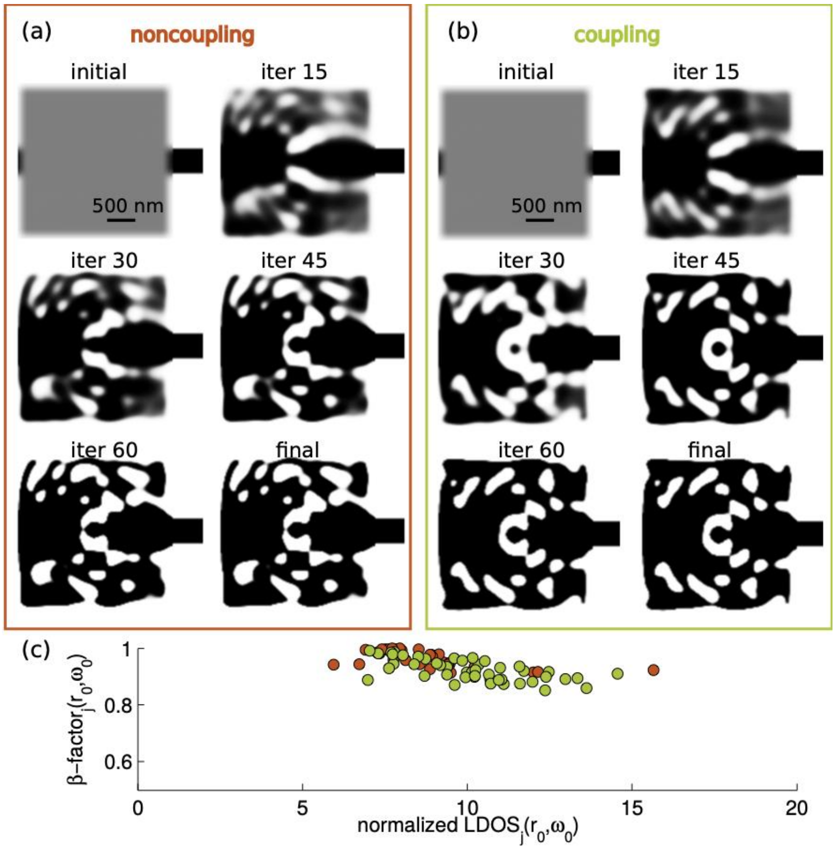

Figure 7. Topology optimization of the integrated Janus single photon source. Evolution of the design region for (a) a noncoupling and (b) coupling Janus dipole. (c) Enhancement of the local density of states and collection efficiency corresponding to the optimized photonic structure on one of the topology optimization realizations.

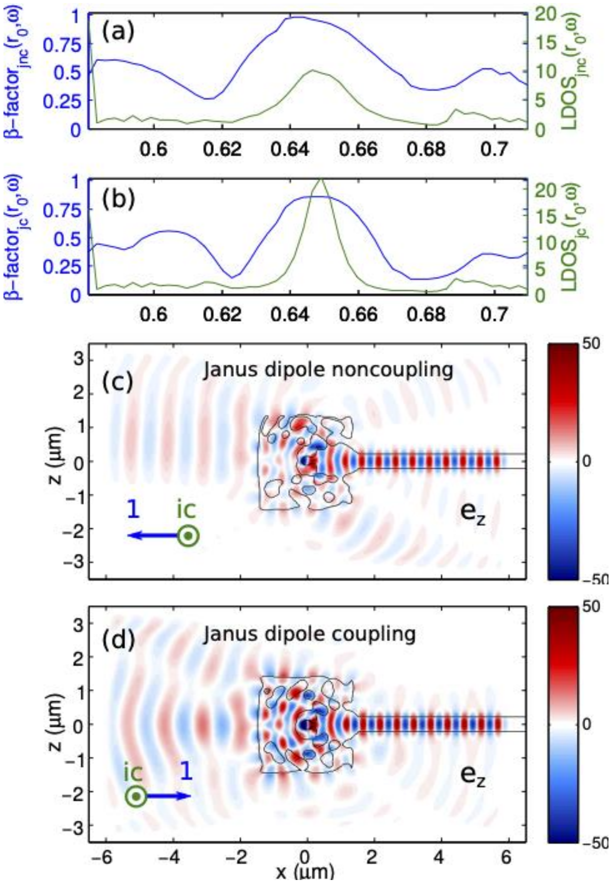

Figure 8. Topology optimization of an integrated Janus single photon source. Purcell- and β- factors spectra at run n = 20 for Janus dipole (a) noncoupling and (b) coupling. Distribution of the electric fields along the topology optimized integrated source. Propagation of the real part of the y-component of the Janus dipole (c) noncoupling and (d) coupling. The inset in (c) and (d) shows the orientation of the Janus dipoles. The frequency is 0.64516(a/λ).

The Janus dipole has orthogonal electric and magnetic dipoles with a π/2 rad phase shift. According to the positive or negative phase shift, the emission couples either into the radiative modes (i.e., Janus noncoupling) or into the guided modes (i.e., Janus coupling) when placed near a waveguide. We calculated that the coupling efficiency of a coupling Janus dipole placed at the center of the topology optimized region is more than one order of magnitude higher than that of the coupling Janus dipole placed in the near field of a waveguide, with an enhancement of about 25 at frequency 0.64516(a/λ) (Fig. S15h). For the noncoupling Janus dipole, the enhancement is more than 1200 times. The topology optimization strategy produces the region that allows a noncoupling Janus dipole to couple its emission into the guided mode. Similarly, in the Janus dipole, the p_x and h_y components of the dipole couple to the e_x and h_y components of the available modes. In optimized design, the topology is formed such that the field modes, specifically the component e_x and h_y have a fixed amplitude and phase relationship. The emission is therefore coupled to the forward and backward modes. Also, the optimization generates a focusing structure on the output waveguide, maximizing the collection efficiency. A collection efficiency of 70% was obtained for a 3D simulation with the effective 2D optimization (2D TO then 3D simulation with the geometry extruded in the vertical direction) and a Purcell factor of 17.

Conclusion

Topology optimization strategies were used to find the best geometries that can increase not only the coupling efficiency of dipole emission radiation into a desired photonic mode but also to enhance the local density of states (LDOS). Linear and circular polarized dipoles placed in small topology-optimized photonic structures (i.e., design region of 3 µm x 3 µm) were used. We demonstrated a mean coupling efficiency and LDOS enhancement higher than 0.86 and 7.2, respectively, for circular polarized, Huygens, and Janus dipoles. In addition, the coupling efficiency of circular polarized, Huygens, and Janus dipoles placed at the center of a topology optimized region is more than one order of magnitude higher than that of the same dipoles placed in the near field of a waveguide. The approach adopted to design 3D photonic device by the extrusion of the optimization design into the vertical direction simplifies the optimization process for fabrication with planar technologies. For practical applications, it is important to use quantum emitters with physical size lower than the volume of a nearby optical field mode in the optimized photonic structure to consider the emitter as a point-like dipole. We expect to extend our approach to other integrated photonic material platforms such as silicon nitride and silicon carbide integrated photonics.

References

[1] G. R. Steinbrecher, J. P. Olson, D. Englund, and J. Carolan. Quantum optical neural networks. npj Quantum Information, 5(1):60, 2019.

[2] C.-Y. Lu and J.-W. Pan. Quantum-dot single-photon sources for the quantum internet. Nature Nanotechnology, 16(12):1294–1296, 2021.

[3] N. Somaschi, et al., Near-optimal single-photon sources in the solid state. Nature Photonics, 10(5):340–345, 2016.

[4] M. Kianinia, Z.-Q. Xu, M. Toth, and I. Aharonovich. Quantum emitters in 2D materials: Emitter engineering, photophysics, and integration in photonic nanostructures. Appl. Phys. Rev., 9(1):011306, 2022.

[5] F. Peyskens, C. Chakraborty, M. Muneeb, D. Van Thourhout, and D. Englund. Integration of single photon emitters in 2D layered materials with a silicon nitride photonic chip. Nature Communications, 10(1):4435, 2019.

[6] E. M. Purcell. Spontaneous emission probabilities at radio frequencies. Phys. Rev., 69(11 and 12), 1946.

[7] J. E. Fröch, S. Kim, N. Mendelson, M. Kianinia, M. Toth, and I. Aharonovich. Coupling hexagonal boron nitride quantum emitters to photonic crystal cavities. ACS Nano, 14(6):7085–7091, 06 2020.

[8] M. Arcari, I. Söllner, A. Javadi, S. Lindskov Hansen, S. Mahmoodian, J. Liu, H. Thyrrestrup, E. H. Lee, J. D. Song, S. Stobbe, and P. Lodahl. Near-unity coupling efficiency of a quantum emitter to a photonic crystal waveguide. Physical Review Letters, 113(9):093603–, 08 2014.

[9] J. Olthaus, P. P. J. Schrinner, D. E. Reiter, and C. Schuck. Optimal photonic crystal cavities for coupling nanoemitters to photonic integrated circuits. Adv. Quantum Technol., 3(2):1900084, 2020.

[10] G. Kirsanske, H. Thyrrestrup, R. S. Daveau, C. L. Dreeßen, T. Pregnolato, L. Midolo, P. Tighineanu, A. Javadi, S. Stobbe, R. Schott, A. Ludwig, A. D. Wieck, S. I. Park, J. D. Song, A. V. Kuhlmann, I. Söllner, M. C. Löbl, R. J. Warburton, and P. Lodahl. Indistinguishable and efficient single photons from a quantum dot in a planar nanobeam waveguide. Physical Review B, 96(16):165306–, 10 2017.

[11] R. Uppu, F. T. Pedersen, Y. Wang, C. T. Olesen, C. Papon, X. Zhou, L. Midolo, S. Scholz, A. D. Wieck, A. Ludwig, and P. Lodahl. Scalable integrated single-photon source. Science Advances, 6(50):eabc8268, 2020.

[12] J. Beltran Madrigal, R. Tellez-Limon, F. Gardillou, D. Barbier, W. Geng, C. Couteau, R. Salas-Montiel, and S. Blaize. Hybrid integrated optical waveguides in glass for enhanced visible photoluminescence of nanoemitters. Applied Optics, 55(36):10263–10268, 2016.

[13] S. Kumar and S. I. Bozhevolnyi. Single photon emitters coupled to plasmonic waveguides: A review. Adv. Quantum Technol., 4(10):2100057, 2021.

[14] S. Molesky, Z. Lin, A. Y. Piggott, W. Jin, J. Vucković, and A. W. Rodriguez. Inverse design in nanophotonics. Nature Photonics, 12(11):659–670, 2018.

[15] Picardi, M.F., Neugebauer, M., Eismann, J.S. et al. Experimental demonstration of linear and spinning Janus dipoles for polarisation- and wavelength-selective near-field coupling. Light Sci Appl 8, 52 (2019). https://doi.org/10.1038/s41377-019-0162-x

[16] J. S. Jensen and O. Sigmund. Topology optimization for nano-photonics. Laser & Photon. Rev., 5(2):308– 321, 2011.

[17] S. Chakravarthi, P. Chao, C. Pederson, S. Molesky, A. Ivanov, K. Hestroffer, F. Hatami, A. W. Rodriguez, and K.-M. C. Fu. Inverse-designed photon extractors for optically addressable defect qubits. Optica, 7(12):1805–1811, 2020.

[18] R. A. Wambold, Z. Yu, Y. Xiao, B. Bachman, G. Jaffe, S. Kolkowitz, J. T. Choy, M. A. Eriksson, R. J. Hamers, and M. A. Kats. Adjoint-optimized nanoscale light extractor for nitrogen-vacancy centers in diamond. 10(1):393–401, 2022-10-06 2021.

[19] O. Yesilyurt, Z. A. Kudyshev, A. Boltasseva, V. M. Shalaev, and A. V. Kildishev. Efficient topology-optimized couplers for on-chip single-photon sources. ACS Photonics, 8(10):3061–3068, 10 2021.

[20] M. F. Picardi, A. V. Zayats, and F. J. Rodríguez-Fortuño. Janus and Huygens dipoles: Near-field directionality beyond spin-momentum locking. Phys. Rev. Lett., 120(11):117402–, 03 2018.

[21] A. Espinosa-Soria and A. Martínez, "Transverse Spin and Spin-Orbit Coupling in Silicon Waveguides," in IEEE Photonics Technology Letters, vol. 28, no. 14, pp. 1561-1564, 15 July15, 2016, doi: 10.1109/LPT.2016.2553841.

[22] Michela F. Picardi, Cillian P. T. McPolin, Jack J. Kingsley-Smith, Xudong Zhang, Shumin Xiao, Francisco J. Rodríguez-Fortuño, and Anatoly V. Zayats, "Integrated Janus dipole source for selective coupling to silicon waveguide networks", Appl. Phys. Rev. 9, 021410 (2022) https://doi.org/10.1063/5.0085487

[23] A. F. Oskooi, D. Roundy, M. Ibanescu, P. Bermel, J. D. Joannopoulos, and S. G. Johnson. Meep: A flexible free-software package for electromagnetic simulations by the FDTD method. Computer Physics Communications, 181(3):687–702, 2010.

[24] J. Kischkat, S. Peters, B. Gruska, M. Semtsiv, M. Chashnikova, M. Klinkmüller, O. Fedosenko, S. Machulik, A. Aleksandrova, G. Monastyrskyi, Y. Flores, and W. T. Masselink. Mid-infrared optical properties of thin films of aluminum oxide, titanium dioxide, silicon dioxide, aluminum nitride, and silicon nitride, Appl. Opt. 51, 6789-6798 (2012).

[25] K. Joulain, R. Carminati, J.-P. Mulet, and J.-J. Greffet. Definition and measurement of the local density of electromagnetic states close to an interface. Phys. Rev. B, 68:245405, 2003.

[26] A. Oskooi and S. G. Johnson. Advances in FDTD computational electrodynamics: photonics and nanotechnology, chapter 4, pages 78, Eq. (4.22). Artech House, Boston - London, 2013.

[27] S. G. Johnson and J. D. Joannopoulos. Block-iterative frequency-domain methods for Maxwell’s equations in a planewave basis. Optics Express, 8(3):173–190, 2001.

[28] K. S. Chiang, "Dual effective-index method for the analysis of rectangular dielectric waveguides," Appl. Opt. 25, 2169-2174 (1986).

[29] Krister Svanberg, "A class of globally convergent optimization methods based on conservative convex separable approximations," SIAM J. Optim. 12 (2), p. 555-573 (2002).

[30] Steven G. Johnson, The NLopt nonlinear-optimization package, http://github.com/stevengj/nlopt.

[31] Alec M. Hammond, Ardavan Oskooi, Mo Chen, Zin Lin, Steven G. Johnson, and Stephen E. Ralph, "High-performance hybrid time/frequency-domain topology optimization for large-scale photonics inverse design," Opt. Express 30, 4467-4491 (2022).

[32] K. Y. Bliokh, A. Y. Bekshaev, and F. Nori. Extraordinary momentum and spin in evanescent waves. Nature Communications, 5(1):3300, 2014.

[33] K. Y. Bliokh and F. Nori. Transverse and longitudinal angular momenta of light. Physics Reports, 592:1–38, 2015.

[34] D. R. Abujetas and J. Sánchez-Gil. Spin angular momentum of guided light induced by transverse confinement and intrinsic helicity. ACS Photonics, 7(2):534–545, 02 2020.

Acknowledgments

We conducted the calculation with the resources of the French regional Grand-Est HPC Center ROMEO.

Funding

We thank the China Scholarship Council File No. 202 008 070 054 for partial financial support. We conducted this work within the frame of the Graduate School (Ecole Universitaire de Recherche) “NANO-PHOT,” contract ANR-18-EURE-0013.

Disclosures

The authors declare no conflicts of interest.

Data availability

Data underlying the results presented in this paper are not publicly available at this time but may be obtained from the authors upon reasonable request.

Supplemental document

Dispersion relation in a 3-µm-thick vertical slab waveguide. Intrinsic properties of eigenmodes in waveguides. Comparison between non-optimized and topology optimized regions. Influence of the design region size and dipole position on the collection efficiency for the circularly polarized dipole. Three-dimensional (3D) topology-optimized photonic device. More results for individual electric and magnetic dipoles oriented along three different axis l = x, y, and z.